5928 *Inorg. Chem.* **2009**, *48*, 5928–5937
DOI: 10.1021/ic900276g

Inorganic Chemistry
Article

Comparative Activities of Nickel(II) and Zinc(II) Complexes of Asymmetric [NN′O] Ligands as 26S Proteasome Inhibitors

Michael Frezza,[†] Sarmad Sahiel Hindo,[‡] Dajena Tomco,[‡] Marco M. Allard,[‡] Qiuzhi Cindy Cui,[†] Mary Jane Heeg,[‡] Di Chen,[†] Q. Ping Dou,*[,†] and Cláudio N. Verani*[,‡]

[†]*The Prevention Program, Barbara Ann Karmanos Cancer Institute, and Department of Pathology, School of Medicine, Wayne State University, Detroit, Michigan 48201, and* [‡]*Department of Chemistry, Wayne State University, 5101 Cass Ave. Detroit, Michigan 48202*

Received February 10, 2009

In this study, we compare the proteasome inhibition capabilities of two anticancer candidates, $[Ni(L^{IA})_2]$ (**1**) and $[Zn(L^{IA})_2]$ (**2**), where L^{IA-} is the deprotonated form of the ligand 2,4-diiodo-6-(((2-pyridinylmethyl)amino)methyl) phenol. Species **1** contains nickel(II), a considerably inert ion that favors covalency, whereas **2** contains zinc(II), a labile transition metal ion that favors predominantly ionic bonds. We report on the synthesis and characterization of **1** and **2** using various spectroscopic, spectrometric, and structural methods. Furthermore, the pharmacological effects of **1** and **2**, along with those of the salts $NiCl_2$ and $ZnCl_2$, were evaluated in vitro and in cultured human cancer cells in terms of their proteasome-inhibitory and apoptotic cell-death-inducing capabilities. It is shown that neither $NiCl_2$ nor **1** have the ability to inhibit the proteasome activity at any sustained levels. However, $ZnCl_2$ and **2** showed superior inhibitory activity versus the chymotrypsin-like activity of both the 26S proteasome (IC_{50} = 5.7 and 4.4 μmol/L, respectively) and the purified 20S proteasome (IC_{50} = 16.6 and 11.7 μmol/L, respectively) under cell-free conditions. Additionally, inhibition of proteasomal activity in cultured prostate cancer cells by **2** was associated with higher levels of ubiquitinated proteins and apoptosis. Treatment with either the metal complex or the salt was relatively nontoxic toward human normal cells. These results strengthen the current working hypothesis that fast ligand dissociation is required to generate an $[ML^{IA}]^+$ pharmacophore, capable of interaction with the proteasome. This interaction, possibly via N-terminal threonine amino acids present in the active sites, renders the proteasome inactive. Our results present a compelling rationale for **2** along with its gallium(III) and copper(II) congeners to be further investigated as potential anticancer drugs that act as proteasome inhibitiors.

Introduction

The use of platinum-containing analogues has been a viable therapeutic strategy in a host of malignancies.[1−5] However, excessive toxicity has hampered their widespread use, leading to the investigation of other metal complexes and distinctive cellular apoptotic pathways.[6,7]

The 26S proteasome has gained substantial consideration as an anticancer target,[8−12] and proteasomal inhibition is a mechanism for tumor cell suppression currently being investigated in our groups. The main function of the ubiquitin−proteasome pathway is to degrade damaged or misfolded proteins.[13,14] Targeted proteins are tagged with a series of ubiquitin molecules which are then translocated to the 26S proteasome and subsequently degraded.[15,16] The enzymatic activity of the 26S proteasome is mediated by the 20S proteasome core that contains three pairs of catalytic

*To whom correspondence should be addressed. Phone: 313 576 8301. Fax: 313 576 8307. E-mail: doup@karmanos.org (Q.P.D.). Phone: 313 577 1076. Fax: 313 577 8022. E-mail: cnverani@chem.wayne.edu (C.N.V.).

(1) Guo, Z.; Sadler, P. J. *Angew. Chem., Int. Ed.* **1999**, *38*, 1512.
(2) Wong, E; Giandomenico, C. M. *Chem. Rev.* **1999**, *99*, 2451.
(3) Wang, D.; Lippard, S. J. *Nat. Rev. Drug Discovery* **2005**, *4*, 307.
(4) Choi, S.; Vastag, L.; Larrabee, Y. C.; Personick, M. L.; Schaberg, K. B.; Fowler, B. J.; Sandwick, R. K.; Rawji, G. *Inorg. Chem.* **2008**, *47*, 1352.
(5) Egger, A. E.; Hartinger, C. G.; Hamidane, H. B.; Tsybin, Y. O.; Keppler, B. K.; Dyson, P. J. *Inorg. Chem.* **2008**, *47*, 10626.
(6) Galanski, M; Arion, V. B.; Jakupec, M. A.; Keppler, B. K. *Curr. Pharm. Des.* **2003**, *9*, 2078.
(7) Ronconi, L.; Giovagnini, L.; Marzano, C.; Bettìo, F.; Graziani, R.; Pilloni, G.; Fregona, D. *Inorg. Chem.* **2005**, *44*, 1867.
(8) Giovagnini, L.; Sitran, S.; Montopoli, M.; Caparrotta, L.; Corsini, M.; Rosani, C.; Zanello, P.; Dou, Q. P.; Fregona, D. *Inorg. Chem.* **2008**, *47*, 6336.
(9) Cvek, B.; Milacic, V.; Taraba, J.; Dou, Q. P. *J. Med. Chem.* **2008**, *51*, 6256.
(10) Adsule, S.; Barve, V.; Chen, D.; Ahmed, F.; Dou, Q. P.; Padhye, S.; Sarkar, F. H. *J. Med. Chem.* **2006**, *49*, 7242.
(11) Beenen, M. A.; An, C.; Ellman, J. A. *J. Am. Chem. Soc.* **2008**, *130*, 6910.
(12) Paramore, A.; Frantz, S. *Nat. Rev. Drug Discovery* **2003**, *2*, 611.
(13) Peters, J. M.; Franke, W. W.; Kleinschmidt, J. A. *J. Biol. Chem.* **1994**, *269*, 7709.
(14) Goldberg, A. L. *Science* **1995**, *268*, 522.
(15) Dou, Q. P.; Li, B. *Drug Res. Update* **1999**, *2*, 215.
(16) Hochstrasser, M. *Cur. Opin. Cell Biol.* **1995**, *7*, 215.

Published on Web 06/04/2009

sites responsible for its chymotrypsin-, trypsin-, and caspase-like activities.[17,18]

The validation of the proteasome as a target for cancer therapy came with the FDA approval of bortezomib for the treatment of multiple myeloma.[19,20] Studies have shown that bortezomib exerts its antitumor effects by binding and deactivating an N-terminal threonine of the chymotrypsin-like active center. Furthermore, other proteasome inhibitors, such as peptide derivatives with aldehydes, sulfones, and epoxyketones,[21] have been shown to be effective in the inactivation of the 26S proteasome by similar mechanisms. Such inhibition has been a valuable approach toward cancer therapy, because it has been shown that human cancer cells are more sensitive to proteasome inhibition than normal cells.[22,23]

We have demonstrated that 2:1 complexes $[M(L^{IA})_2]$, with [NN′O] ligands and gallium(III) or copper(II), can promote proteasome inhibition in prostate cancer[24,25] and cisplatin-resistant neuroblastoma cells.[26] The mechanisms of inhibition are not entirely clear and could involve the deactivation of either the 19S terminal caps or the 20S core. Nonetheless, molecular modeling with similar complexes suggests that such species cannot dock into the proteasome satisfactorily, indicating that new bonds between the inhibitor and the 20S core must be established. Experimental results with equivalent copper(II) species suggest that a 1:1 pharmacophore $[M(L^{IA})]^+$ (or an aqua equivalent) is needed to allow coordination with the terminal threonine or other coordinating residues.[24,25] Thus, an equilibrium $[M(L^{IA})_2] \leftrightarrow [M(L^{IA})]^+ + L^{IA-}$ for 2:1 species seems necessary. Therefore, we aim at furthering these studies by designing similar $[M(L^{IA})_2]$ complexes using divalent nickel(II) and zinc(II) metals. Differences due to electronic configurations of the metals lead to species with characteristic behavior for ligand dissociation, as depicted in Scheme 1. Nickel(II) has a $3d^8$ configuration, which leads to nonzero ligand-field stabilization energies (LFSE) and, consequently, should foster slow ligand dissociation, whereas zinc(II) with a $3d^{10}$ configuration has zero LFSE, thus fostering rapid ligand dissociation.[27−29] Slow ligand dissociation would therefore give rise to poor inhibition because no deactivation of the proteasomal active core takes place.

Scheme 1. Suggested Equilibrium of $[M(L^{IA})_2] \leftrightarrow [M(L^{IA})]^+ + L^{IA-}$ to Generate the $[M(L^{IA})]^+$ Pharmacophore

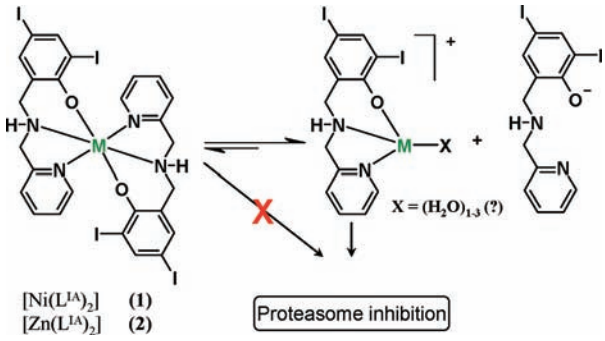

In this paper, we report on the synthesis and characterization of $[Ni(L^{IA})_2]$ (**1**) and $[Zn(L^{IA})_2]$ (**2**) using various spectroscopic, spectrometric, and structural methods. After careful characterization, these species were evaluated as proteasome inhibitors to the purified 20S proteasome and 26S proteasome in whole-cell extracts, as well as in intact prostate cancer and leukemia cells. The results follow.

Results and Discussion

Ligand Design. Our groups are interested in the development of discrete complexes of well-established stoichiometry, formed between asymmetric [NN′O] ligands and transition metal ions for anticancer therapy. Such ligands are an evolution from terbutylated analogues used as biomimetic models for galactose−oxidase.[30] The presence of electron-donating and -withdrawing phenol substituents (i.e., H, ^{t}Bu, Cl, Br, and I) in such complexes has shown a distinctive influence on the apoptosis of cisplatin-resistant neuroblastoma and prostate cancer cell lines.[25,26] We are mostly engaged with the phenol-based ligand 2,4-diiodo-6-(((2-pyridinylmethyl)amino)methyl)phenol, synthesized by treatment of 2-hydroxy-3,5-diiodobenzaldehyde with 2-aminomethylpyridine followed by reduction with sodium borohydride.[26] Upon deprotonation, this ligand leads to 2:1 ligand-to-metal $[M(L^{IA})_2]$ species with divalent ions, hence, eliminating the required charge balance by counterions. Moreover, a secondary amine in this ligand allows for the design of species with appended moieties to enhance water solubility[31,32] (currently at 4.5×10^{-5} mol/L for the

(17) Seemuller, E; Lupas, A.; Stock, D.; Lowe, J.; Huber, R.; Baumeister, W. *Science* **1995**, *268*, 579.
(18) Voges, D.; Zwickl, P.; Baumeister, W. *Annu. Rev. Biochem.* **1999**, *68*, 1015.
(19) Dou, Q. P.; Goldfarb, R. H. *IDrugs* **2002**, *5*, 828.
(20) Kane, R. C.; Farrell, A. T.; Sridhara, R.; Pazdur, R. *Clin. Cancer Res.* **2006**, *12*, 2955.
(21) (a) Borissenko, L.; Groll, M. *Chem. Rev.* **2007**, *107*, 687. (b) Kisselev, A. F.; Goldberg, A. L. *Chem. Biol.* **2001**, *08*, 739. (c) McCormack, T. A.; Cruikshank, A. A.; Grenier, L.; Melandri, F. D.; Nunes, S. L.; Plamondon, L.; Stein, R. L.; Dick, L. R. *Biochemistry* **1998**, *37*, 7792.
(22) Adams, J.; Palombella, V. J.; Sausville, E. A.; Johnson, J.; Destree, A.; Lazarus, D. D.; Maas, J.; Pien, C. S.; Prakash, S.; Elliott, P. J. *Cancer Res.* **1999**, *59*, 2615.
(23) An, B.; Goldfarb, R. H.; Siman, R.; Dou, Q. P. *Cell Death Differ.* **1998**, *5*, 1062.
(24) Hindo, S. S.; Frezza, M.; Tomco, D.; Heeg, M. J.; Hryhorczuk, L.; McGarvey, B. R.; Dou, Q. P.; Verani, C. N. *Eur. J. Med. Chem.* **2009**, accepted.
(25) Chen, D.; Frezza, M.; Shakya, R.; Cui, Q. C.; Milacic, V.; Verani, C. N.; Dou, Q. P. *Cancer Res.* **2007**, *67*, 9258.
(26) Shakya, R.; Peng, F.; Liu, J.; Heeg, M. J.; Verani, C. N. *Inorg. Chem.* **2006**, *45*, 6263.
(27) See, for example: (a) Miessler, G. L.; Tarr, D. A. *Inorganic Chemistry*, 3rd ed.; Pearson-Prentice Hall: Upper Saddle River, NJ, 2004; Chapter 12, pp 412−453. (b) Basolo, F.; Pearson, R. G. Mechanisms of Inorganic Reactions; 2nd ed.; John Wiley & Sons: New York, 1967; Chapter 3, pp.124−246.
(28) Sekaly, A. L. R.; Murimboh, J.; Hassan, N. M.; Mandal, R.; Ben Younes, M. E.; Chakrabarti, C. L.; Back, M. H. *Environ. Sci. Technol.* **2003**, *37*, 68.
(29) (a) Johnson, D. A.; Nelson, P. G. *Inorg. Chem.* **1995**, *34*, 5666. (b) Johnson, D. A.; Nelson, P. G. *Inorg. Chem.* **1995**, *34*, 3253.
(30) (a) Michel, F.; Thomas, F.; Hamman, S.; Philouze, C.; Saint-Aman, E.; Pierre, J.-L. *Eur. J. Inorg. Chem.* **2006**, *I-18*, 3684. (b) Shimazaki, Y.; Huth, S.; Odani, A.; Yamauchi, O. *Angew. Chem., Int. Ed.* **2000**, *39*, 1666. (c) Itoh, S.; Taki, M.; Takayama, S.; Nagatomo, S.; Kitagawa, T.; Sakurada, N.; Arakawa, R.; Fukuzumi, S. *Angew. Chem., Int. Ed.* **1999**, *38*, 2774. (d) Neves, A.; Verani, C. N.; de Brito, M. A.; Vencato, I.; Mangrich, A.; Oliva, G.; Souza, D. D. H. F.; Batista, A. A. *Inorg. Chim. Acta* **1999**, *290*, 207. (e) Vaidyanathan, M.; Viswanathan, R.; Palaniandavar, M.; Balasubramanian, T.; Prabhaharan, P.; Muthiah, T. P. *Inorg. Chem.* **1998**, *37*, 6418. (f) Zurita, D.; Gautier-Luneau, I.; Ménage, S.; Pierre, J.-L.; Saint-Aman, E. *J. Biol. Inorg. Chem.* **1997**, *2*, 46.
(31) (a) Storr, T.; Sugai, Y.; Barta, C. A.; Mikata, Y.; Adam, M. J.; Yano, S.; Orvig, C. *Inorg. Chem.* **2005**, *44*, 2698. (b) Melchior, M.; Rettig, S. J.; Liboiron, B. D.; Thompson, K. H.; Yuen, V. G.; McNeill, J. H.; Orvig, C. *Inorg. Chem.* **2001**, *40*, 4686. (c) Clevette, D. J.; Nelson, W. O.; Nordin, A.; Orvig, C.; Sjoeberg, S. *Inorg. Chem.* **1989**, *28*, 2079.
(32) Lord, S. J.; Epstein, N. A.; Paddock, R. L.; Vogels, C. M.; Hennigar, T. L.; Zaworotko, M. J.; Taylor, N. J.; Driedzic, W. R.; Broderick, T. L.; Westcott, S. A. *Can. J. Chem.* **1999**, *77*, 1249.

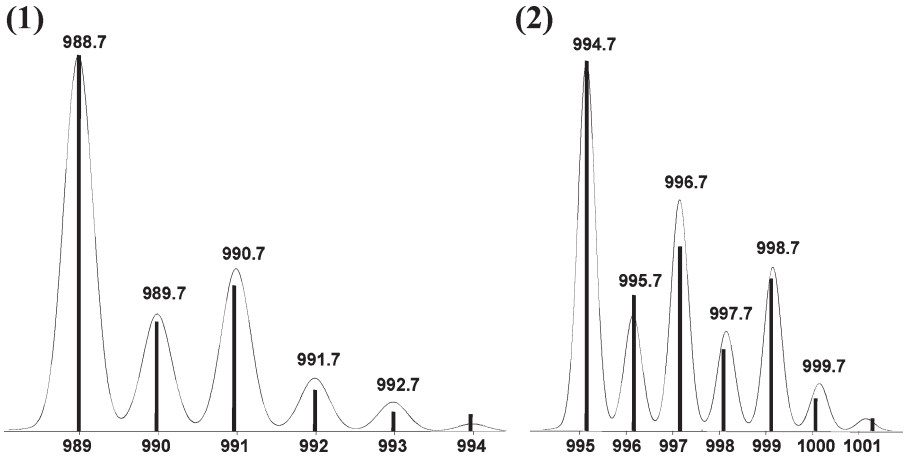

Figure 1. ESI(pos) peak clusters for $[\mathbf{1}+(H^+)]^+$ and $[\mathbf{2}+(H^+)]^+$ in methanol. The relative abundance axis of each complex is omitted for clarity.

equivalent gallium complex[26]) or lipophilicity.[33−36] Such changes can address concerns with future oral administration as therapeutics.

Syntheses, Spectrometric, and Spectroscopic Evaluation. Complexes $[Ni(L^{IA})_2]$ (**1**) and $[Zn(L^{IA})_2]$ (**2**) were synthesized by treatment of HL^{IA} with the proper acetate salts in methanol and were isolated in good yields (∼80%). Triethylamine was used as a base to ensure ligand deprotonation. Spectrometric evaluation of **1** and **2** in methanol using electrospray ionization mass spectrometry (ESIMS) in the positive mode led to identification with a good isotopic distribution for the main peaks, m/z = 988.7 and 994.7, respectively, for $[\mathbf{1}+(H^+)]^+$ and $[\mathbf{2}+(H^+)]^+$ (Figure 1). The 1:1 ligand-to-metal species were also detected via ESIMS. Since such species only become prominent at higher cone voltages, they were considered a direct result of the fragmentation of **1** and **2**. Infrared spectra confirmed the presence of the ligand and revealed the absence of peaks at ca. 1560 and 1450 cm^{-1} associated with potential acetate counterions. This gives further evidence that the 2:1 ligand-to-metal species are the favored products. Furthermore, elemental analyses were in excellent agreement with those expected for **1** and **2**.

The ^1H NMR spectrum of the ligand shows the expected signals for protons at the pyridine and phenol rings between 7.0 and 9.0 ppm.[26] Distinctive signals for methylene groups vicinal to the pyridine and phenol rings appear respectively as singlet peaks at 3.94 and 3.91 ppm. At room temperature, the ^1H NMR spectrum of the zinc complex **1** is comparable to that of the ligand with further splitting of the peaks between 7 and 9 ppm, suggestive of two ligands with dissimilar conformations. Equally distinctive is the observation that the methylene signals become broadened and split into six ill-defined bands, indicating that the complex is not rigid[37] and that at least six of the eight methylene protons are nonequivalent. By lowering the temperature to ca. −60 °C, these signals coalesce into three peaks. The amine proton, originally at 3.49 ppm in the ligand, splits into two broad peaks at 1.77 and 1.18 pm and appears at 2.20 ppm at low temperatures. The nickel species yielded broad and ill-defined ^1H NMR results, in agreement with the paramagnetic nature of a $3d^8$ high-spin species. A detailed investigation of the ligand dynamics[38] of **1** and its gallium-containing counterpart[26] using VT-NMR properties is under development.

Molecular Structural Characterization. Good crystals for X-ray diffractometric analyses were isolated for **1** and **2** in chloroform and dichloromethane, respectively, and their molecular structures were determined. The ORTEP renditions for **1** and **2** are shown in Figure 2, and selected bond lengths and angles are displayed in Table 1. Complex **1** crystallizes in a monoclinic space group $P2_1/n$ composed of a nickel(II) ion coordinated to two deprotonated $(L^{IA})^-$ ligands, with each of them containing an $[N_{py}N_{am}O_{phen}]$ set of donors. Both ligands are facially coordinated with the two pyridine rings ($Ni-N_{py} \approx 2.09$ Å), the two amine groups ($Ni-N_{am} \approx 2.09$ Å), and the two phenolate rings ($Ni-O_{phen} \approx 2.04$ Å), arranged trans to one another to yield a pseudo-octahedral geometry. Crystals of **2** appeared as colorless needles and crystallize in an orthorhombic $P2_12_12_1$ space group, also showing a similar facial coordination of the $(L^{IA})^-$ ligands in a pseudo-octahedral geometry. However, whereas **1** exhibits a symmetrical all-trans environment described as $[Ni<N_{am1}N_{am2}><N_{py1}N_{py2}><O_{(phO-)1}O_{(phO-)2}>]$[39] in a bent arrangement,[36] **2** is described as having an all-cis $[Zn<N_{am1}O_{(phO-)2}><N_{py1}N_{am2}><O_{(phO-)1}N_{py2}>]$. As observed by the ^1H NMR spectrum with distinctive signals for methylene groups, the two ligands present dissimilar conformations.

We have demonstrated the role played by structural and electronic effects in a series of $3d^{5-10}$ $[M(L)_2]$ species with such asymmetric NN′O ligands. Although ligand rigidity enforces *meridional* coordination in similar imine

(33) (a) Kirin, S. I.; Dübon, P.; Weyhermu1ller, T.; Bill, E.; Metzler-Nolte, N. *Inorg. Chem.* **2005**, *44*, 5405. (b) Kirin, S. I.; Happel, C. M.; Hrubanova, S.; Weyhermüller, T.; Klein, C.; Metzler-Nolte, N. *Dalton Trans.* **2004**, 1201.

(34) Shakya, R.; Imbert, C.; Hratchian, H. P.; Lanznaster, M.; Heeg, M. J.; McGarvey, B. R.; Allard, M.; Schlegel, H. B.; Verani, C. N. *Dalton Trans.* **2006**, 2517.

(35) Shakya, R.; Hindo, S. S.; Wu, L.; Allard, M. M.; Heeg, M. J.; Hratchian, H. P.; McGarvey, B. R.; Da Rocha, S. R. P.; Verani, C. N. *Inorg. Chem.* **2007**, *46*, 9808.

(36) Lesh, F. D.; Hindo, S. S.; Heeg, M. J.; Allard, M. M.; Jain, P.; Peng, B.; Hryhorczuk, L.; Verani, C. N. *Eur. J. Inorg. Chem.* **2009**, 345.

(37) Mugesh, G.; Singh, H. B.; Butcher, R. J. *Eur. J. Inorg. Chem.* **2001**, 669.

(38) Coggin, D. K.; Gonzalez, J. A.; Kook, A. M.; Stanbury, D. M.; Wilson, L. J. *Inorg. Chem.* **1991**, *30*, 1115.

(39) The notation $<A_1B_2>$ indicates that A is trans to B, with A and B corresponding to the pyridine (Npy), amine (Nam), or phenolato (OphO−) donors. Subscripts 1 and 2 designate the first or the second ligand.

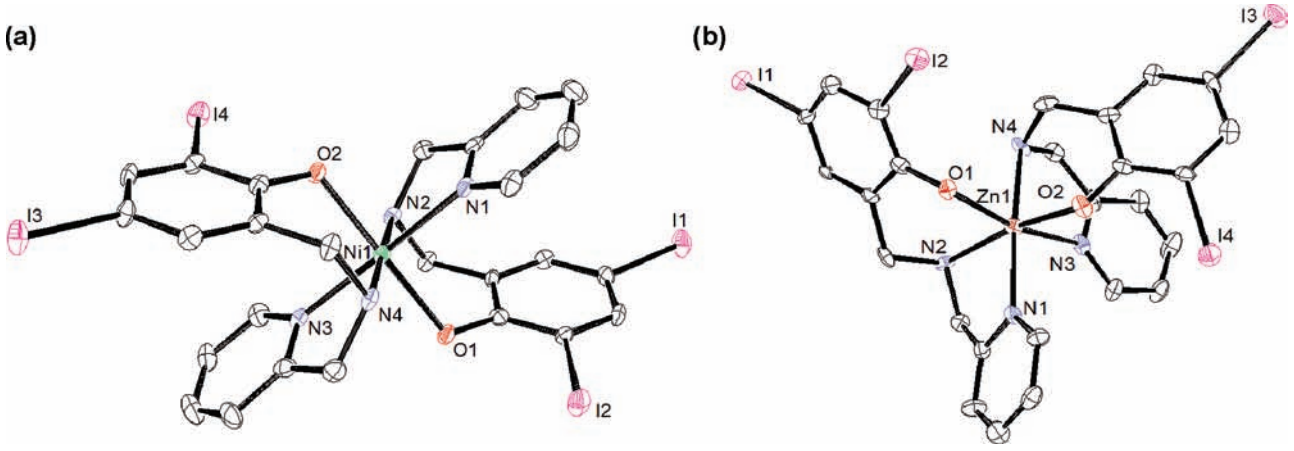

Figure 2. ORTEP diagrams at 50% probability level for **1** (a) and **2** (b).

Table 1. Selected Bond Lengths (Å) and Angles (deg) for **1** and **2**

1	**2**
Ni(1)−O(2) = 2.036(2)	Zn(1)−O(2) = 2.025(6)
Ni(1)−O(1) = 2.057(2)	Zn(1)−O(1) = 2.111(5)
Ni(1)−N(2) = 2.088(3)	Zn(1)−N(1) = 2.149(6)
Ni(1)−N(3) = 2.090(3)	Zn(1)−N(4) = 2.179(6)
Ni(1)−N(4) = 2.096(3)	Zn(1)−N(2) = 2.181(7)
Ni(1)−N(1) = 2.098(3)	Zn(1)−N(3) = 2.259(7)
O(2)−Ni(1)−O(1) = 179.52(10)	O(2)−Zn(1)−O(1) = 92.0(2)
O(2)−Ni(1)−N(2) = 87.86(10)	O(2)−Zn(1)−N(1) = 90.0(2)
O(1)−Ni(1)−N(2) = 91.99(10)	O(1)−Zn(1)−N(1) = 99.6(2)
O(2)−Ni(1)−N(3) = 89.60(10)	O(2)−Zn(1)−N(4) = 92.4(2)
O(1)−Ni(1)−N(3) = 90.87(10)	O(1)−Zn(1)−N(4) = 88.7(2)
N(2)−Ni(1)−N(3) = 99.14(11)	N(1)−Zn(1)−N(4) = 171.3(3)
O(2)−Ni(1)−N(4) = 92.66(10)	O(2)−Zn(1)−N(2) = 168.9(2)
O(1)−Ni(1)−N(4) = 87.49(10)	O(1)−Zn(1)−N(2) = 89.2(2)
N(2)−Ni(1)−N(4) = 179.47(11)	N(1)−Zn(1)−N(2) = 79.0(2)
N(3)−Ni(1)−N(4) = 80.76(11)	N(4)−Zn(1)−N(2) = 98.6(2)
O(2)−Ni(1)−N(1) = 88.86(10)	O(2)−Zn(1)−N(3) = 87.9(2)
O(1)−Ni(1)−N(1) = 90.66(10)	O(1)−Zn(1)−N(3) = 166.7(2)
N(2)−Ni(1)−N(1) = 81.01(11)	N(1)−Zn(1)−N(3) = 93.7(2)
N(3)−Ni(1)−N(1) = 178.45(11)	N(4)−Zn(1)−N(3) = 78.1(3)
N(4)−Ni(1)−N(1) = 99.10(12)	N(2)−Zn(1)−N(3) = 93.5(2)

ligands, electronic configuration leads to a *facial* coordination mode in flexible amines. The metal centers also dictate the preferential cis or trans orientation of equivalent phenolates and other donor sets in vicinal ligands, with $3d^5_{\text{high-spin}}$ ions[40] displaying a cis arrangement and $3d^6_{\text{low-spin}}$ and $3d^7_{\text{high-spin}}$ ions[36,37] supporting a trans orientation. Species **1** reinforces[38] the notion of an all-trans mode for $3d^8$ configurations, whereas **2** seems to fall within other $3d^{10}$ configurations[26,41−43] lacking a clear preference. Another remark is that, while most of the $O_{\text{phenolate}}$ bond lengths for **1** and **2** are comparable at 2.02−2.05 Å, one of the $Zn-O_{\text{phenolate}}$ bonds for **2** is elongated, reaching ca. 2.11 Å. This longer bond length is comparable to values found in the literature.[44] This is attributed to the $3d^{10}$ electronic configuration of the zinc (II) ion, which favors electrostatic interactions.

Electronic Structure Calculations. A series of electronic structure calculations were carried out for the nickel-containing **1** and zinc-containing **2**, as well as on isomers with alternative geometries and binding modes, aiming at evaluating bond nature, delocalization, and energy differences between isomers. These results allowed for gaining insight on how the electronic structure of these species may foster the formation of the expected pharmacophores $[ML^{IA}]^+$. The optimized geometries for the electronic structures of **1** and **2** are in good agreement with the crystallographic data presented above.

Nickel Species. A recent study by Thomas et al.[45] on similar nickel complexes supports a favorable trans facial coordination of the ligands over the *meridional* mode by approximately 5.0 kcal/mol using a comparable level of theory. Therefore, we restricted our studies to two different all-trans *facial* isomers, namely, the structurally characterized **1** and a hypothetical **1′**. Isomer **1** displays both phenolate rings in parallel planes, whereas these same rings are perpendicular to one another in **1′** (Figure 3A). The energy difference between the two structures is 3.7 kcal/mol, clearly favoring **1** as the lowest energy state. Interestingly, we recently compared similar isomers with unsubstituted phenolate rings,[38] and the energy difference was a mere 1.1 kcal/mol. It can be suggested that the iodine substituents play a significant role in favoring **1** instead of **1′**. Furthermore, both isomers display triplet ground states with $S = 1$, consistent with a $3d^8$ high-spin configuration where two unpaired electrons populate the $d_{x^2-y^2}$ (SOMO) and d_{z^2} (SOMO−1) orbitals (Figure 3B).

Because divalent zinc is a $3d^{10}$ ion, it lacks LFSE, and the coordination mode is most likely the result of ligand sterics. For **2**, we observed a new facial all-cis $[Zn < N_{am1}O_{(phO-)2} > < N_{py1}N_{am2} > < O_{(phO-)1}N_{py2} >]$ coordination mode for a doubly deprotonated species, well in contrast with the all-trans counterpart obtained by Neves et al.[43] with a nonsubstituted ligand. Thus, two different facial isomers were explored for the zinc complex, as shown in Figure 4A: the structurally characterized **2** and a hypothetical **2′** that matched the geometry

(40) Imbert, C.; Hratchian, H. P.; Lanznaster, M.; Heeg, M. J.; Hryhorczuk, L. M.; McGarvey, B. R.; Schlegel, H. B.; Verani, C. N. *Inorg. Chem.* **2005**, *44*, 7414.
(41) Lanznaster, M.; Neves, A.; Vencato, I.; Bortoluzzi, A. J.; Gallardo, H.; Machado, S. P.; Assumpcao, A. M. C. *J. Braz. Chem. Soc.* **2006**, *17*, 289.
(42) Neves, A.; Vencato, I.; Verani, C. N. *J. Braz. Chem. Soc.* **1997**, *8*, 265.
(43) dos Anjos, A.; Bortoluzzi, A. J.; Szpoganicz, B.; Caro, M. S. B.; Friedermann, G. R.; Mangrich, A. S.; Neves, A. *Inorg. Chim. Acta* **2005**, *358*, 3106.
(44) Cotton, F. A.; Daniels, L. M.; Murillo, C. A.; Quesada, J. F. *Inorg. Chem.* **1993**, *32*, 4861.
(45) Rotthaus, O.; Labet, V.; Philouze, C.; Jarjayes, O.; Thomas, F. *Eur. J. Inorg. Chem.* **2008**, 4215.

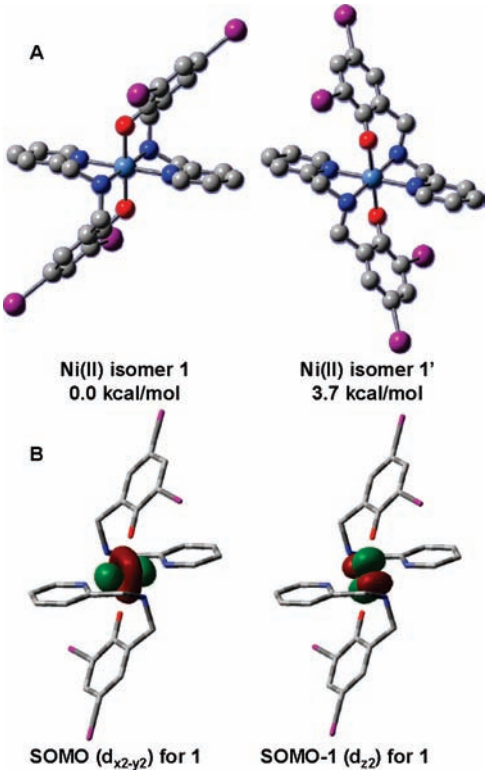

Figure 3. (A) Depiction of the two facial $[Ni(L^{IA})_2]$ isomers **1** and **1′**. (B) Selected MOs for unpaired electrons.

adopted for the nickel-containing **1**. Interestingly, the calculations favor **2′** by a small margin of less than 2.0 kcal/mol, thus, in disagreement with the observed structure. Therefore, in the absence of a LFSE, the bonding is mainly ionic in nature, and other factors such as solvation, crystal packing, or intermolecular force effects must control the final geometry.

In order to address partial atomic charges, natural bond order (NBO) analysis was performed with both **1** and **2**; the results are shown in Table 2. It is clear from these charge distributions that the interaction between the Ni(II) center in **1** and the ligand is more delocalized, that is, covalent, than the interaction between the Zn(II) center and the ligand in **2**. This can be seen by lower charges on the metal: 1.3 for **1** versus 1.6 for **2**. The values for other atoms in **2** are consistently larger in magnitude, reinforcing the notion of more localized, that is, ionic, bonds. These values indicate that there is less stabilization of the positive divalent metal charge onto the ligands for **2** over **1**. This difference is significant, since both complexes are discrete neutral species with an overall zero charge. Thus, it is possible to conclude that an ionic nature would favor ligand dissociation in the biologic milieu for **2**, and the equilibrium suggested in Scheme 1 should be facilitated.

Finally, initial theoretical treatment of the possible binding modes between the fragment $[Zn(L^{IA})]^+$ and a deprotonated threonine residue were also performed. A simplified $[Zn(L)]^+$ fragment with an unsubstituted ligand was used, and in order to model the terminal nature of the threonine residue, a dimethylated amide residue was incorporated, as shown in Figure 4B. Two coordination modes were probed: the first considered

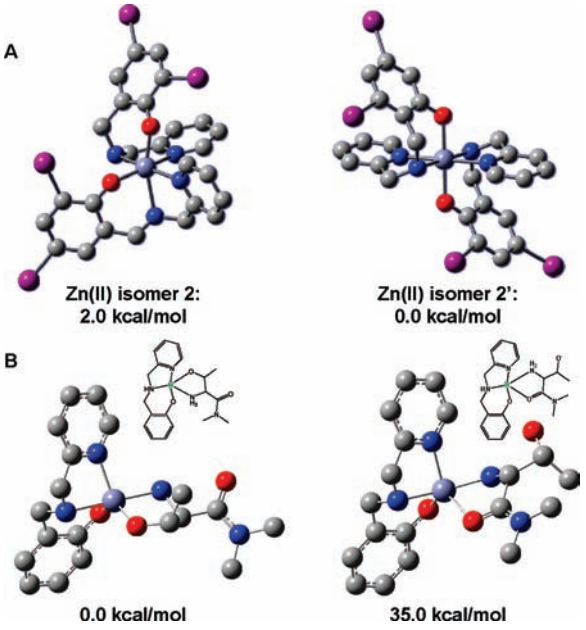

Figure 4. (a) Depiction of the two facial $[Zn(L^{IA})_2]$ isomers **2** and **2′**. (b) Possible interaction between the fragment $[Zn(L^{IA})]^+$ and threonine.

Table 2. NBO Partial Atomic Charges

	Ni (**1**)	Zn (**2**)
M	1.3	1.6
O1	−0.87	−0.90
O2	−0.87	−0.92
N1	−0.56	−0.64
N2	−0.75	−0.77
N3	−0.56	−0.61
N4	−0.75	−0.80

binding between the zinc center at the $[Zn(L)]^+$ fragment with the terminal (and deprotonated) hydroxyl group and the secondary amine group, whereas the second focused on the binding through the secondary amine and the carbonyl group of the amide residue. The first binding mode is approximately 35 kcal/mol more stable, and although this proposition is merely speculative at this point, it suggests that terminal hydroxo/amine coordination to zinc would be favored.

Induction of Cell Death and Inhibition of Cell Proliferation. The cytotoxic effects of $NiCl_2$, $ZnCl_2$, **1**, and **2** were tested in human leukemia Jurkat T cells treated at different concentrations for 18 h. After each treatment, a trypan blue exclusion assay was performed to assess cell death (Figure 5A). Cells treated with **2** exhibited a dose-dependent activity reaching 48%, 70%, 95%, and 100% cell death at 7.5, 10, 15, and 20 μmol/L, respectively. This turned to be the single viable species, since the metal salts and **1** had marginal cell-death induction, smaller than ~10% compared with DMSO-treated cells, at as high as 20 μmol/L.

To substantiate this effect further, we evaluated whether **2** can suppress cell proliferation of human prostate cancer cells. C4-2B human prostate cancer cells were treated with $NiCl_2$, $ZnCl_2$, **1**, **2**, and the DMSO control at different concentrations for 18 h, followed by measurement of cell proliferation by MTT assay (Figure 5B). It was observed that cells treated with **2** suppressed cell

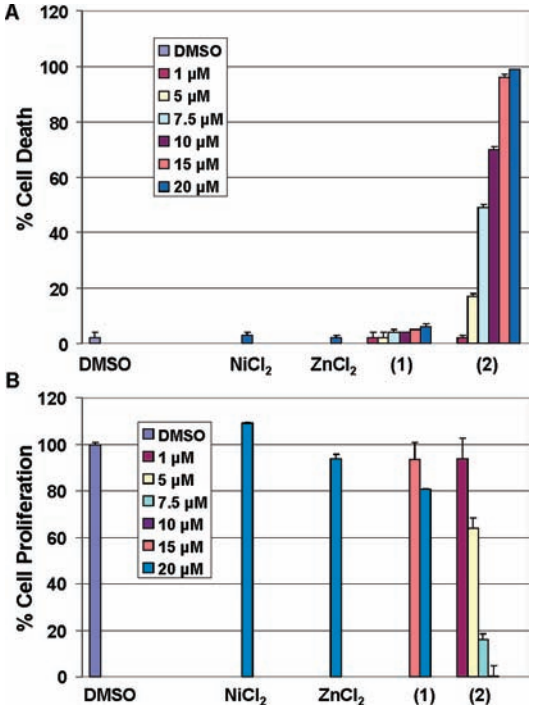

Figure 5. Cell death (A) and cell growth inhibition (B) on human leukemia and prostate cancer cells by $NiCl_2$, $ZnCl_2$, **1**, and **2**.

proliferation in a dose-dependent manner (IC_{50} = ~6 μmol/L), reaching 100% inhibition at 10 μmol/L. Furthermore, cells treated with **2** at 5 and 7.5 μmol/L decreased cell proliferation by ~35% and ~85%, respectively. Consistently, C4-2B cells treated with the metal salts or **1** showed little or no inhibitory effect, even at the highest concentration tested of 20 μmol/L.

***In Vitro* Proteasome Inhibition.** To test the proteasome inhibitory capacity of these species, a comparison of the inhibitory activity of $NiCl_2$, $ZnCl_2$, **1**, and **2** to the 26S proteasomal activity was performed under cell-free conditions. An extract of C4-2B prostate cancer cells (Figure 6A) was used, and the results indicate that both the $ZnCl_2$ salt and **2** have the potential to inhibit the chymotrypsin-like activity of the 26S proteasome with IC_{50} values of 5.7 and 4.4 μmol/L, respectively. This result is consistent with our previous finding that zinc dithiocarbamate complexes can target and inhibit the proteasome.[46] However, extracts treated with **1** at as high as 25 μmol/L showed only ~20% inhibition on the 26S proteasome, suggesting that intrinsic distinctive mechanisms of inhibition must be present for **1** and **2**. Consistent with this finding is the fact that $NiCl_2$ at 25 μmol/L could only inhibit the proteasomal activity by ~25%.

To provide direct evidence for distinct mechanisms, we incubated a purified rabbit 20S proteasome with $NiCl_2$, $ZnCl_2$, **1**, and **2** at various concentrations, followed by measurement of the chymotrypsin-like activity (Figure 6B). We found that this activity was significantly inhibited with the salt $ZnCl_2$ and **2** with similar potencies (IC_{50} = 16.6 and 11.7 μmol/L, respectively). Although $NiCl_2$ showed modest inhibitory activity, **1** was rather inactive. Overall, our data remain consistent with the fact that the zinc ion,

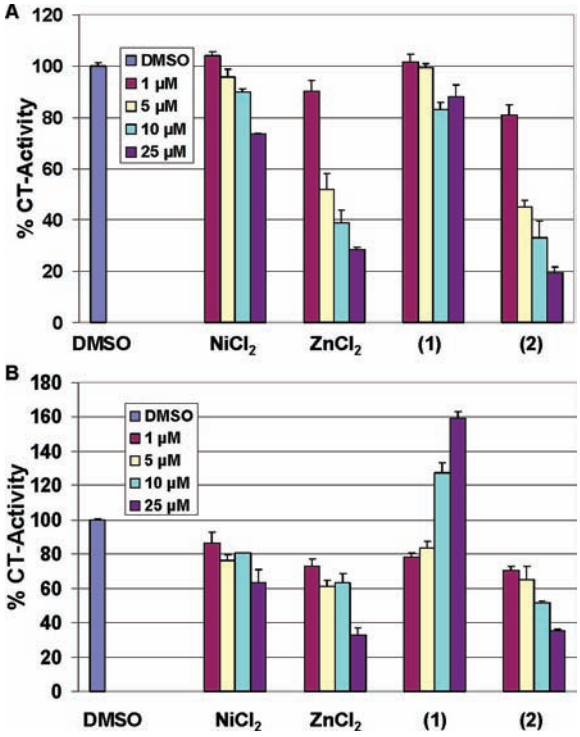

Figure 6. *In vitro* proteasome-inhibitory activity of $NiCl_2$, $ZnCl_2$, **1**, and **2**. (A) Inhibition of CT-like activity of 26S proteasome in C4-2B cell extract. (B) Inhibition of the CT-like activity of purified 20S protesome.

both as a chloride salt and a complex with the $(L^{IA})^-$ ligand, is able to target and inhibit the proteasome under cell-free conditions.

Proteasome Inhibition and Apoptosis Induction in Intact Cancer Cells. To confirm the ability of **2** to inhibit the proteasomal activity in intact tumor cells, C4-2B human prostate cancer cells were first treated with different concentrations (5, 10, and 25 μmol/L) of $NiCl_2$, $ZnCl_2$, **1**, and **2** for 18 h, followed by measurement of proteasome inhibition. The values for proteasomal chymotrypsin-like activity are given as a percentage in Table 3. The C4-2B cells treated with **2** showed a dose-dependent inhibition of the proteasomal activity of 31% inhibition at 10 μmol/L and an 86% inhibition at 25 μmol/L. Consistently, levels of ubiquitinated proteins were increased in a dose-dependent manner in C4-2B cells (Figure S1, Supporting Information). In comparison, cells treated with either $NiCl_2$, $ZnCl_2$, or **1** showed negligible proteasome inhibitory effect.

It has been shown that proteasome inhibition can lead to decreased levels of androgen receptor (AR) expression.[47,48] Therefore, a decrease in such expression should be observed assuming proteasome activity inhibition by **2**. Consistently, this is the only species that down-regulated significantly AR, and 25 μmol/L treatment completely abrogated AR expression levels (Figure S1, Supporting Information). These results remain consistent with the ability of **2** to inhibit the proteasome activity.

It has been shown that inhibition of the proteasomal chymotrypsin-like activity selectively in transformed cells

(46) Milacic, V.; Chen, D.; Giovagnini, L.; Diez, A.; Fregona, D.; Dou, Q. P. *Toxicol. App. Pharm.* **2008**, *231*, 24.

(47) Lin, H. K.; Altuwaijri, S.; Lin, W. J.; Kan, P. Y.; Collins, L. L.; Chang, C. *J. Biol. Chem.* **2002**, *277*, 36570.

(48) Yang, H. J.; Murthy, S.; Sarkar, F. H.; Sheng, S.; Reddy, G. P. V.; Dou, Q. P. *J. Cell. Physiol.* **2008**, *217*, 569.

Table 3. Percentile of CT-Activity after Treatment with $NiCl_2$, $ZnCl_2$, **1**, and **2**

	dose, μM	C4-2B, %	SD[a](+/−)	PC3%	SD[a](+/−)	MCF 10A %	SD (+/−)
DMSO		100	0.81	100	1.56	100	3.00
$NiCl_2$	25	92	1.41	99	0.10	98	1.83
$ZnCl_2$	25	99	0.90	127	0.45	116	1.56
	5	84	0.87	101	0.01		
$[Ni(L^{IA})_2]$ (**1**)	10	83	0.96	81	1.59		
	25	80	2.27	92	0.85	89	1.96
	5	111	1.02	114	2.63	118	0.55
$[Zn(L^{IA})_2]$ (**2**)	10	69	0.14	17	1.38	97	1.48
	25	14	0.68	10	1.13	83	1.59

[a] Standard deviation.

could result in the induction of apoptosis.[23] To investigate whether proteasome inhibition and androgen receptor down-regulation are associated with apoptotic cell death, apoptotic-specific poly-ADP-ribose polymerase (PARP) disappearance and morphological changes were measured in the same experiment (Figure 7, Figure S1, Supporting Information). The results show that only cells treated with 25 μmol/L of **2** were able to completely abrogate full-length PARP, whereas cells treated with either $NiCl_2$, $ZnCl_2$, or **1** at the highest concentration tested had little visible effects. Consistently, morphological changes (detached, shrunken, and apoptotic blebbing) were observed in cells treated with 25 μmol/L of **2** and to a significant but lesser extent at 10 μmol/L (Figure 7). Much fewer aberrant morphological changes were detected in the cells treated with metal salt or **1** at the highest concentration tested (Figure 7). These results show that the induction of apoptosis in C4-2B cells by **2** is associated with inhibition of the proteasomal chymotrypsin-like activity.

Upon demonstrating the ability of **2** to inhibit the proteasomal chymotrypsin-like activity in AR-dependent C4-2B prostate cancer cells, we then tested the effect of **2** on AR-independent PC-3 human prostate cancer cells. PC-3 cells were treated with 5, 10, and 25 μmol/L of **1** or **2** and their metal salt for 18 h, followed by measurement of the proteasome activity, accumulated levels of ubiquitinated proteins, and apoptosis induction. The percentage of proteasomal chymotrypsin-like activity is designated in Table 3 with DMSO as a control. We found that **2** could inhibit the proteasomal activity and induce apoptotic cell death in PC-3 prostate cancer cells, whereas **1**, $NiCl_2$, and $ZnCl_2$ showed little or no effect (Table 3, Figure S2).

Kinetics of Proteasome Inhibition and Apoptosis Induction. To study the kinetic effect of proteasome inhibition, C4-2B prostate cancer cells were treated with 15 μmol/L of **2** over different time points (2−18 h), and their cell lysates were used to measure the proteasomal-chymotrypsin-like activity (Figure 8A). The proteasomal chymotrypsin-like activity was inhibited by 18%, 42%, 57%, and 63% respectively at 2, 4, 8, and 18 h. This result was consistent with the time-dependent increase in levels of accumulated ubiquitinated proteins. Furthermore, lower levels of AR were detected in cells treated with **2** at all time points, and complete abrogation of AR expression is detected in cells after 18 h of treatment. Importantly, apoptosis-specific PARP down-regulation was detected at later time points, with complete PARP disappearance at 18 h (Figure S3, Supporting Information). Apoptosis induction at later time points is also typified with the appearance of aberrant morphological changes (detached, shrunken, and apoptotic blebbing; Figure 8B). These results clearly demonstrate that induction of the apoptosis occurs after proteasome inhibition. Thus, proteasome inhibition appears to be required for apoptosis induction.

Tumor Cell Selectivity. The ability to distinguish normal from malignant cells is of paramount importance for

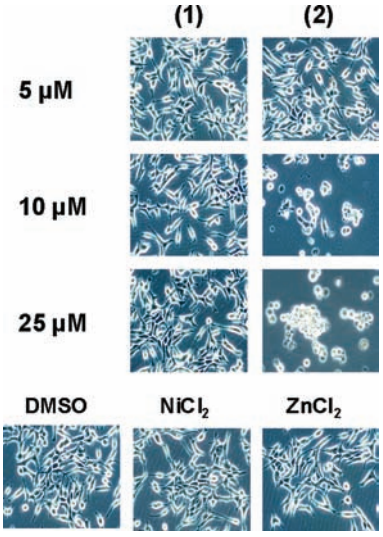

Figure 7. Cellular morphological effects of $NiCl_2$, $ZnCl_2$, **1**, and **2** on C4-2B prostate cancer cells.

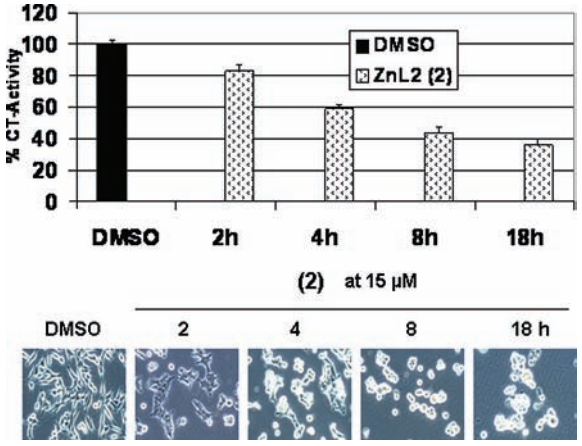

Figure 8. Kinetic effect of proteasome inhibition and apoptosis induction by **2** in C4-2B prostate cancer cells.

developing clinically relevant anticancer drugs. To determine whether inhibition of prostate cancer cellular proteasome activity achieved by **2** is selective toward malignant cells but not normal cells, we used normal-immortalized human breast cell line MCF-10A. The MCF-10A cells were treated with different concentrations of **2** as high 25 μmol/L for 18 h, followed by measurement of proteasomal chymotrypsin-like activity and apoptosis. We found that when these nontransformed cells were treated with **2**, only 17% proteasome inhibition was detected at the highest concentrations tested (Table 3). Other treatments also had little effect on MCF-10A cells (Table 3). To determine whether the inability of **2** to inhibit the proteasome activity at sustainable levels is associated with the lack of apoptosis induction in these normal immortalized breast cells, apoptosis-associated morphological changes were then assessed in the same experiment. These normal, immortalized MCF-10A cells showed only little such cell-death-related detachment after treatment with **2** up to 18 h at the highest concentration tested (Figure S4, Supporting Information). Furthermore, the species $NiCl_2$, $ZnCl_2$, and **1** had little or no cytotoxic effect on normal cells. Our data suggest that **2** could inhibit the proteasome activity and induce apoptosis selectively in human cancer cells but not in normal immortalized cells, validating **2** as a promising proteasome inhibitor.

Summary and Conclusions

In this paper, we report on two new coordination complexes as potential anticancer candidates, namely, $[Ni(L^{IA})_2]$ (**1**) and $[Zn(L^{IA})_2]$ (**2**). Both species were characterized by several spectroscopic, spectrometric, and structural methods and display a well-established 2:1 ligand-to-metal stoichiometry. DFT calculations considering different isomers of **1** and **2** were performed and show good agreement with the nickel species but fail to predict the appropriate geometry for the zinc-containing species. Furthermore, initial studies considering coordination of a 1:1 $[Zn(L)]^+$ fragment with threonine suggest a favorable coordination through the terminal hydroxyl group of the amino acid.

The effects of $NiCl_2$, $ZnCl_2$, **1**, and **2** were tested toward a purified rabbit 20S proteasome and 26S proteasome in cell extracts (in which cell membranes have been disrupted) of leukemia and human prostate cancer cell lines. The results indicate that only **2** and $ZnCl_2$ have a direct inhibitory effect on the proteasome to any significant level. Furthermore, when $NiCl_2$, $ZnCl_2$, **1**, and **2** were tested on the 26S proteasome of cultured intact leukemia and human prostate cancer cells, it was evidently shown that only **2** exhibited potent antiproliferative and cell-death-inducing activity. Similarly, only **2** induced higher levels of ubiquitinated proteins, which were associated with decreased levels of proteasomal chymotrypsin-like activity. In addition, the decrease of proteasomal chymotrypsin-like activity observed for **2** is tightly associated with tumor cell apoptosis, as seen by the morphological changes and the apparent disappearance of the full-length PARP fragment. Species **2** also showed remarkably low cytotoxicity toward normal human breast cells.

This sharp contrast in proteasome activity inhibition between **1** and **2** is suggested to be related to the nature of the metal ion and its degree of reactivity when combined with NN′O-containing ligands. As observed in similar complexes from our group,[24] considerable proteasome inhibition can be attained through 1:1 ligand-to-metal species that is believed to be the pharmacophore in all of these species. Therefore, an equilibrium $[M(L^{IA})_2] \leftrightarrow [M(L^{IA})]^+ + L^{IA-}$ seems necessary to facilitate the formation of the pharmacophore with available coordination sites capable of interaction with the 20S proteasome, likely to be via the N-terminal threonine residue. It is observed from the molecular structures and DFT calculations available that covalent interactions prevail in **1**, while **2** is ionic in nature. We, therefore, propose that this intrinsic difference defines the facility of pharmacophore formation and determines the activity of these species. The lack of activity observed for $ZnCl_2$ in intact cells reinforces the notion offered for the equivalent copper counterparts[24] that the ligand $(L^{IA})^-$ serves as a shuttle vector to cross the cellular membrane. Taken together, we suggest that the presence of the fragment $[Zn(L^{IA})]^+$ is required for proteasome inhibition. At this point, it is not clear whether the ligand dissociation $[Zn(L^{IA})_2] \leftrightarrow [Zn(L^{IA})]^+ + L^{IA-}$ is intra- or extracellular, and, if intracellular, before or after reaching the 26S proteasome. Furthermore, it is likely that water molecules will coordinate to the zinc ion, forming $[Zn(L^{IA})(H_2O)_n]^+$ hydrated species. The investigation of these issues is a current goal of our groups and will be properly developed in the future. Nonetheless, the data observed thus far provide a compelling rationale for the clinical development of **2** as a potential anticancer drug.

Experimental Section

Materials and Methods. All reagents were obtained from commercial sources and were used as received. Methanol was distilled over CaH_2. IR spectra were measured from 4000 to 400 cm^{-1} as KBr pellets on a Tensor 27 FTIR spectrophotometer. ESI spectra in the positive mode were measured in methanol on a Micromass Quattro LC triple quadrupole mass spectrometer with an electrospray/APCI source and a Walters Alliance 2695 LC autosampler and photodiode array UV detector. Experimental assignments were simulated on the basis of peak location and isotopic distributions. The ^1H NMR spectra were measured in $CDCl_3$ on a Varian Unity-300 instrument. Elemental analyses were performed by Midwest Microlab, Indianapolis, Indiana. Trypan blue exclusion dye was purchased from Sigma Aldrich (St. Louis, MO). The peptide substrate Suc-LLVY-AMC (for the proteasomal chymotrypsin-like activity) was purchased from Calbiochem, Inc. (San Diego, CA). RPMI 1640, penicillin, and streptomycin were purchased from Invitrogen (Carlsbad, CA). Fetal bovine serum was purchased from Aleken Biologicals (Nash, TX). Antibodies against ubiquitin, actin, and secondary antibodies were purchased from Santa Cruz Biotechnology (Santa Cruz, CA). Mouse monoclonal antibody against human PARP was purchased from BIOMOL International LP (Plymouth Meeting, PA).

X-Ray Structural Determination for $[Ni(L^{IA})_2]$ (1) and $[Zn(L^{IA})_2]$ (2). Diffraction data were measured on a Bruker X8 APEX-II κ geometry diffractometer with Mo radiation and a graphite monochromator. Frames were recorded for 10 s at 100 K with the detector at 40 mm and 0.3° between each frame. APEX-II[49] and SHELX[50] software were used in the collection and refinement of the models (Table 4).

Crystals of $[Ni(L^{IA})_2]$ (**1**) were colorless plates. A total of 86 456 reflections were counted, which averaged to 10 883

(49) APEX II collection and processing programs are distributed by the manufacturer: *APEX II*; Bruker AXS Inc.: Madison WI, 2005.

(50) Sheldrick, G. M. *Acta Crystallogr.* **2008**, *A64*, 112–122.

Table 4. Crystal Data and Structure Refinements for $[Ni(L^{IA})_2]$ (**1**) and $[Zn(L^{IA})_2]$ (**2**)

formula	$C_{29}H_{25}C_{19}I_4N_4O_2Ni$	$C_{29}H_{30}C_{16}I_4N_4O_3Zn$
fw	1346.89	1268.24
space group	$P2_1/n$	$P2_12_12_1$
a (Å)	18.4231(5)	13.2593(4)
b (Å)	10.1797(3)	15.4882(5)
c (Å)	22.1493(6)	19.6143(6)
β (deg)	92.8120(10)	
V (Å^3)	4148.9(2)	4028.0(2)
Z	4	4
temp (K)	100(2)	100(2)
λ (Å)	0.71073	0.71073
density, calcd (Mg cm^{-3})	2.156	2.091
μ (mm^{-1})	4.057	4.109
R(F) (%)[a]	3.63	6.33
Rw(F) (%)[a]	5.91	13.18

[a] $R(F) = \sum||F_o| - |F_c||/\sum|F_o|$; $Rw(F) = [\sum w(F_o^2 - F_c^2)^2/\sum w(F_o^2)^2]^{1/2}$ for $I > 2\sigma(I)$.

independent data. Hydrogen atoms were placed at calculated positions except for those on nitrogen which were observed. The complex crystallized with 3 equiv of chloroform. All atoms occupy general positions.

Crystals of $[Zn(L^{IA})_2]$ (**2**) appeared as colorless needles. A total of 77 377 reflections were measured, yielding 14 112 unique data. Hydrogen atoms were placed in calculated positions. The complex crystallized with 3 equiv of methylene chloride and 1 equiv of water. All atoms occupy general positions.

Electronic Structure Calculation Methods. The B3LYP level of theory[51] with the SDD[52] basis sets was employed throughout because of the presence of iodine atoms, and all of the calculations were done using the Gaussian[53] series of programs. Geometries were fully minimized, without symmetry constraints, using standard methods.[54] Located stationary points were characterized by computing analytic vibrational frequencies. Reported energies include zero-point correction. Cartesian coordinates of all of the optimized structures are provided in the Supporting Information.

Syntheses. The iodo-substituted ligand HL^{IA} was synthesized by the treatment of 2-hydroxy-3,5-diiodobenzaldehyde with 2-aminomethylpyridine in methanol followed by reduction with sodium borohydride, as previously published.[26]

$[Ni(L^{IA})_2]$ (1). A 15 mL methanol solution of HL^I (0.49 g, 1.1 mmol) was added dropwise to a 15 mL of a methanol solution of $Ni(OAc)_2 \cdot 2H_2O$ (0.25 g, 1.2 mmol) at 45 °C. After 45 min, a purple precipitate was obtained, isolated by frit filtration, and washed with cold methanol and ether. The solid was recrystallized in chloroform. Yield = 0.95 g (88%). Elem anal. calcd for **1**, $C_{26}H_{22}NiI_4N_4O_2$: C, 31.58; H, 2.24; N, 5.67. Found: C, 31.47; H, 2.30; N, 5.56. IR (KBr, cm^{-1}): 3068 ν(N−H), 1606, 1593 (C=N from pyridine), 1486 (C−O from phenyl). ESI pos. in MeOH: m/z = 988.9 for $[NiL_2 + H^+]^+$.

$[Zn(L^{IA})_2]$ (2). A 15 mL methanol solution containing HL^I (0.51 g, 1.1 mmol) was added dropwise to a 15 mL methanol solution of $Zn(OAc)_2 \cdot 2H_2O$ (0.26 g, 1.2 mmol) at 45 °C. A white precipitate was obtained after 1 h, isolated by frit filtration, and washed with cold methanol and ether. The solid was recrystallized in dichloromethane. Yield = 0.85 g (77%). Elem anal. calcd for **2**, $C_{26}H_{22}ZnI_4N_4O_2$: C, 31.37; H, 2.23; N, 5.63. Found: C, 31.27; H, 2.38; N, 5.58. IR (KBr, cm^{-1}): 3290 (N−H), 1608 (C=N from pyridine), 3079 ν(N−H). ESI pos. in MeOH: m/z = 994.9 for $[ZnL_2 + H^+]^+$.

Cell Cultures and Whole-Cell Extract Preparation. Human prostate cancer cells, C4-2B and PC-3, and human leukemia Jurkat T cells were grown in RPMI-1640 supplemented with 10% fetal bovine serum and maintained at 37 °C and 5% CO_2. MCF-10A (normal, derived from benign human breast tissue) was obtained and cultured as previously described.[55] A whole-cell extract was prepared as previously described.

Cell Proliferation Assay. Cells were seeded in quadruplicate in a 96-well plate and grown until 70−80% confluence was reached, followed by treatment with the indicated agents for 18 h. After that, the 3-(4,5-dimethylthiazol-2-yl)-2,5-diphenyltetrazolium bromide (MTT) assay was done as described previously.

Trypan Blue Assay. Jurkat T cells were treated with $NiCl_2$, $ZnCl_2$, **1**, and **2** for 18 h at the indicated concentrations followed by the measurement of cell death. The trypan blue dye exclusion assay was performed by mixing 100 μL of a cell suspension with 50 μL of 0.4% trypan blue dye before injecting it into a hemocytometer and counting. The number of cells that absorbed the dye and those that excluded the dye were counted, from which the percentage of nonviable cells to total cells was calculated.

Proteasomal Activity in Whole-Cell Extract or Purified 20S Proteasome. C4-2B whole-cell extract (8 μg) or a purified 20S rabbit proteasome (35 ng) was incubated with 10 μmol/L of the CT-substrate, Suc-LLVY-AMC, in 100 μL of the assay buffer [50 mmol/L Tris-HCl (pH 7.5)] in the presence of $NiCl_2$, $ZnCl_2$, **1**, and **2** at various concentrations or solvent DMSO as a control. After 2 h of incubation at 37 °C, the production of hydrolyzed AMC groups was measured using a Wallac Victor3 multilabel counter with an excitation filter of 365 nm and an emission filter of 460 nm.

Proteasome CT-Like Activity in Cells. Proteins extracted from cells after each treatment were incubated for 2 h at 37 °C in 100 μL of the assay buffer (50 mmol/L Tris-HCL, pH 7.5) with 10 μmol/L of the fluorogenic substrate Suc-LLVY-AMC, as described previously.

Western Blot Analysis. Cell extracts were separated by SDS-PAGE and transferred to a nitrocellulose membrane. A western blot analysis was performed using specific antibodies to PARP, ubiquitin, or AR, followed by visualization using the HyGLO reagent (Denville Scientific, Metuchin, NJ).

Cellular Morphology Analysis. A Zeiss Axiovert 25 microscope was used for all microscopic imaging with phase contrast for cellular morphology. Magnification was ×100.

(51) (a) Becke, A. D. *J. Chem. Phys.* **1993**, *98*, 5648. (b) Becke, A. D. *Phys. Rev. A* **1988**, *38*, 3098. (c) Lee, T.; Yang, W. T.; Parr, R. G. *Phys. Rev. B* **1988**, *37*, 785. (d) Gordon, M. S. *Chem. Phys. Lett.* **1980**, *76*, 163. (e) Hariharan, P. C.; Pople, J. A. *Mol. Phys.* **1974**, *27*, 209. (f) Hariharan, P. C.; Pople, J. A. *Theor. Chim. Acta* **1973**, *28*, 213. (g) Hehre, W. R.; Ditchfield, R.; Pople, J. A. *J. Chem. Phys.* **1972**, *56*, 225. (h) Ditchfield, R.; Hehre, W. R.; Pople, J. A. *J. Chem. Phys.* **1971**, *54*, 724.

(52) Dolg, M.; Wedig, U.; Stoll, H.; Preuss, H. *J. Chem. Phys.* **1987**, *86*, 866.

(53) Frisch, M. J.; Trucks, G. W.; Schlegel, H. B.; Scuseria, G. E.; Robb, M. A.; Cheeseman, J. R.; Montgomery, J. A.; Vreven, T.; Kudin, K. N.; Burant, J. C.; Millam, J. M.; Iyengar, S. S.; Tomasi, J.; Barone, V.; Mennucci, B.; Cossi, M.; Scalmani, G.; Rega, N.; Petersson, G. A.; Nakatsuji, H.; Hada, M.; Ehara, M.; Toyota, K.; Fukuda, R.; Hasegawa, J.; Ishida, M.; Nakajima, T.; Honda, Y.; Kitao, O.; Nakai, H.; Klene, M.; Li, X.; Knox, J. E.; Hratchian, H. P.; Cross, J. B.; Bakken, V.; Adamo, C.; Jaramillo, J.; Gomperts, R.; Stratmann, R. E.; Yazyev, O.; Austin, A. J.; Cammi, R.; Pomelli, C.; Ochterski, J. W.; Ayala, P. Y.; Morokuma, K.; Voth, G. A.; Salvador, P.; Dannenberg, J. J.; Zakrzewski, V. G.; Dapprich, S.; Daniels, A. D.; Strain, M. C.; Farkas, O.; Malick, D. K.; Rabuck, A. D.; Raghavachari, K.; Foresman, J. B.; Ortiz, J. V.; Cui, Q.; Baboul, A. G.; Clifford, S.; Cioslowski, J.; Stefanov, B. B.; Liu, G.; Liashenko, A.; Piskorz, P.; Komaromi, I.; Martin, R. L.; Fox, D. J.; Keith, T.; Al-Laham, M. A.; Peng, C. Y.; Nanayakkara, A.; Challacombe, M.; Gill, P. M. W.; Johnson, B.; Chen, W.; Wong, M. W.; Gonzalez, C.; Pople, J. A. *GAUSSIAN 03*; Gaussian, Inc.: Wallingford, CT, 2003.

(54) Schlegel, H. B. *J. Comput. Chem.* **1982**, *3*, 214.

(55) Daniel, K. G.; Chen, D.; Orlu, S.; Cui, Q. C.; Miller, F. R.; Dou, Q. P. *Breast Cancer Res.* **2005**, *7*, R897.

Acknowledgment. M.F. and S.S.H. contributed equally to this publication. QPD acknowledges the Karmanos Cancer Institute of Wayne State University, the Department of Defense Breast Cancer Research Program (W81XWH-04-1-0688 and DAMD17-03-1-0175) and the National Cancer Institute (1R01-CA120009). CNV acknowledges the Wayne State University and partial support from the National Science Foundation (CHE-0718470). M.F. acknowledges a training grant, "Ruth L. Kirschstein National Service Research Award" (T32-CA009531).

Supporting Information Available: This material is available free of charge via the Internet at http://pubs.acs.org.